Astron. Astrophys. 362, 886–894 (2000)

ASTRONOMY AND ASTROPHYSICS

Nonthermal emission from clusters of galaxies

A.M. Bykov[1], **H. Bloemen**[2], **and Yu.A. Uvarov**[1]

[1] A.F. Ioffe Institute for Physics and Technology, St. Petersburg, 194021, Russia
[2] SRON Utrecht, Sorbonnelaan 2, 3584 CA Utrecht, The Netherlands

Received 21 April 2000 / Accepted 31 August 2000

Abstract. We demonstrate that fast moving halos in clusters of galaxies provide a plausible source of (extended) nonthermal X-ray and γ-ray emission. This follows from the fact that accelerated particles are produced in their bow shocks. A substantial fraction of a virialized ensemble of halos can have moderate supersonic velocities outside the central region of a rich cluster. Dark matter halos of supersonic and superalfvenic velocity will create collisionless bow shocks of moderate Mach number $M \gtrsim 2$, due to electromagnetic interaction between comoving baryonic matter and the hot intra-cluster gas. We present kinetic modelling of nonthermal electron injection, acceleration and propagation in such systems and conclude that the halos are efficient electron accelerators and sources of hard X-ray and γ-ray emission. Inverse-Compton radiation, bremsstrahlung, and synchrotron radiation by these electrons produce spectra that are in quantitative agreement with e.g. the hard X-ray and radio emission observed from the Coma cluster. Moreover, the relative increase of hard X-ray emission outside the central 0.3–0.4 Mpc of the cluster A2199, as observed by *BeppoSAX*, can be understood in this framework. Spatially resolved hard X-ray and γ-ray spectra of clusters (e.g. *INTEGRAL*) can determine the contribution of the energetic lepton component generated by supersonic halo motions to the observed nonthermal emission, thus constraining the energetic nuclear component.

Key words: acceleration of particles – radiation mechanisms: non-thermal – galaxies: clusters: general – gamma rays: theory – radio continuum: galaxies – X-rays: galaxies

1. Introduction

Growth of the hierarchical structure of the Universe as the result of merging and accretion of dark matter substructures is a generic feature now of cold dark matter (CDM) cosmogony (e.g. White & Rees 1978). N-body simulations are successfully used to model the clustering evolution (e.g. Frenk et al. 1999; Bertschinger 1999) and provide a generally consistent picture of thermal X-ray emission from clusters. Substantial substructure of dark matter is predicted by modern high-resolution N-body simulations of the evolution of dark matter halos in clusters (e.g. Ghigna et al. 1998; Klypin et al. 1999a; Okamoto & Habe 1999; Moore et al. 1999) as well as galactic halos (e.g. Klypin et al. 1999b; Moore et al. 1999). Rees (1986) proposed that gravitationally-confined gas in dark minihalos may account for the Lyman absorption lines in quasar spectra. Blitz et al. (1999) have suggested recently an elegant link between so called High Velocity Clouds and low-mass ($\gtrsim 10^8 M_\odot$) bound dark-matter clumps in the Local Group.

Clusters of galaxies have long been known to be sources of thermal X-ray emission, but increasing evidence is now being found for a distinct nonthermal component. For the Coma cluster, indications are seen by *EUVE* (Lieu et al. 1996; Bowyer et al. 1999), by *BeppoSAX* (Fusco-Femiano et al. 1999), and by *RXTE* (Rephaeli et al. 1999). *BeppoSAX* has detected hard X-ray emission from the rich clusters A2199 (Kaastra et al. 1999) and A2256 (Fusco-Femiano et al. 2000). For A2199, Kaastra et al. (1999) found from *BeppoSAX* observations that the evidence for nonthermal (hard X-ray) emission is limited to radii $\gtrsim 300$ kpc. Kempner & Sarazin (2000) placed an upper limit on the diffuse radio flux from A2199 and they concluded that this constrains an inverse-Compton origin of the hard X-ray emission. Nonthermal bremsstrahlung may account for the observed flux (see also Sarazin & Kempner 2000) and they noted that the source of fresh accelerated electrons may be shocks generated by motions of galaxies. Turbulent wakes created by galactic motions in an intra-cluster medium (ICM) have long been considered as potential sources of ICM magnetic-field amplification and sites for *in-situ* turbulent acceleration of radio-emitting electrons (e.g. Roland 1981; Schlickeiser et al. 1987). Gamma-ray emission has not yet been detected from clusters (e.g. Rephaeli et al. 1994; Rephaeli & Dermer 1997; Sreekumar et al. 1996; Reimer 1999).

Völk et al. (1996) and Berezinsky et al. (1997) demonstrated that clusters of galaxies are able to keep cosmic rays for a cosmological time scale. They also estimated the diffuse high-energy γ-ray and neutrino production due to the interaction of cosmic rays with the intra-cluster gas. Upper limits imposed by *EGRET* observations of Coma and Virgo (Sreekumar et al. 1996) substantially limit the possibility of cosmic-ray equipartition in clusters (Blasi 1999). Völk & Atoyan (1999) estimated the ICM magnetic field to be $\sim 0.1\,\mu$G and pointed out that such a rela-

Send offprint requests to: A.M. Bykov (byk@astro.ioffe.rssi.ru)

tively weak field would be consistent with an inverse-Compton origin (e.g. Rephaeli 1979) of excessive EUV and hard X-ray emission from the Coma cluster given the radio synchrotron spectrum (see also Hwang 1997; Enßlin & Biermann 1998; Sarazin & Lieu 1998). The required relativistic electrons must have been accelerated recently (less than a few Gyrs ago). An inverse-Compton origin by electrons injected 2 Gyrs ago was advocated by Enßlin et al. (1999). Also Sarazin (1999) concluded that hard X-ray tails and diffuse radio emission are only expected in clusters with recent particle acceleration, e.g. due to merger shocks.

Current models of nonthermal emission from clusters generally deal with *ad hoc* assumed energetic particle populations (see, however, the model of cluster radio emission by Schlickeiser et al. 1987). Our aim here is to examine in detail particle acceleration and nonthermal emission of an ensemble of galactic halos moving supersonically through the ICM. We used the following:

(i) the results of global N-body simulations of the dynamical evolution of galactic halos in rich clusters (Frenk et al. 1999; Okamoto & Habe 1999) to obtain a model of the spatial velocity dispersion distribution of halos;
(ii) the theory of gas stripping of galaxies interacting with the hot ICM as described by Gaetz et al. (1987), Balsara et al. (1994), and Stevens et al. (1999) to model the structure of the halo bow shock;
(iii) the kinetic model of electron injection and acceleration by collisionless shocks from Bykov & Uvarov (1999), accounting for Coulomb losses in the turbulent halo media, to simulate the spectra and distribution of nonthermal electrons.

The local emissivities from bremsstrahlung, inverse-Compton radiation, and synchrotron radiation were calculated as the accelerated electrons evolve through the post-shock structure. After integration over the halo region, the resulting spectra were weighted with the halo velocity distribution function and the mass function of cluster galaxies.

In Sect. 2 we discuss the statistics of fast moving halos that are creating bow shocks. In Sect. 3 we address the energy spectrum of energetic electrons as they pass through the different regions that can be associated with a halo bow shock. In Sect. 4 we present calculations of nonthermal emission by the accelerated electrons. In Sect. 5 we compare our results with observations.

2. Bow shocks of dark matter halos in a cluster

Dark-matter velocity dispersion profiles have been calculated in several N-body simulations (e.g. Frenk et al. 1999; Okamoto & Habe 1999 and references therein). The mass-weighted halo velocity dispersion of a rich cluster ($\sim 10^{15} M_\odot$; $z = 0$) was shown by Okamoto & Habe (1999) to have a distinct radial dependence, as illustrated in Fig. 1a. The profile peaks at 0.3–0.5 Mpc from the cluster center, with a velocity dispersion $\sigma/\sqrt{3}$ of ~ 1000 km s^{-1}. The simulations indicate a low mass-weighted velocity dispersion inside the central $\sim$0.2 Mpc due to dynamical friction and a decreasing velocity dispersion with time after $z \sim 0.2$. Okamoto & Habe also found that after redshift $z \sim 0.5$ more than 60% of the massive ($\gtrsim 10^{11} M_\odot$) halos in the central 0.5 Mpc of a cluster is destroyed and that the fraction of surviving halos has a clear correlation with distance from the cluster center. For the present work, the particularly important basic conclusion to be drawn is that a substantial number of large high-velocity halos is expected outside the central region of clusters with redshifts below 0.2.

The velocity distribution of halos in a cluster depends on dissipative and relaxation processes and has not been studied yet with high-resolution simulations. If the velocity distribution is approximated by a Maxwell distribution with 3D dispersion σ (to be justified by future high-resolution simulations), then the fraction of halos $\phi(v_0)$ having velocities v_h above v_0 can be calculated from:

$$\phi(v_0) = \sqrt{\frac{2}{\pi}} \frac{1}{\sigma^3} \int_{v_0}^{\infty} dv v^2 \exp\left(-\frac{v^2}{2\sigma^2}\right) \quad (1)$$

To estimate the associated Mach numbers one must know the temperature and magnetic field profiles in the cluster. A study of global properties of 207 clusters, based on observations by the *Einstein Observatory*, was performed by White et al. (1997). They present average radial profiles for electron density, baryon fraction, and gas temperature and studied correlations between an average temperature inside the cluster and the optical velocity dispersion. It is important to note here that the measured optical velocity dispersion related to the whole cluster is in general not equal to the mass-weighted halo velocity dispersion derived in N-body simulations. *Only the mass-weighted halo velocity dispersion is important for the model under consideration here. This is due to the fact that electron acceleration is dominated by the most extended (and most massive) supersonically moving halos for a Press-Schechter halo mass distribution.*

The sound speed ($c_s \approx 1700\, T_8^{0.5}$ km s^{-1}) and the Alfvén velocity ($v_a \approx 70\, B_{-6} n_{-3}^{-0.5}$ km s^{-1}) in the ICM imply (sonic) Mach numbers $M_h = v_h/c_s \gtrsim 1$ ($v_a << c_s$) for halos moving with velocity $\gtrsim \sigma$ in a cluster of mass $\sim 10^{15} M_\odot$ as simulated by Okamoto & Habe (1999). Here T_8 is the ICM temperature measured in 10^8 K, B_{-6} is the ICM magnetic field in μG and n_{-3} is the ICM number density measured in 10^{-3} cm^{-3}.

A supersonically (and superalfvenic) moving halo will drive a collisionless bow shock if there is baryonic matter comoving with the halo. The amount of comoving baryonic matter depends upon the balance between ram-pressure stripping and replenishment rates. These effects were subject of hydrodynamical modelling by Gaetz et al. (1987), Balsara et al. (1994), and most recently by Stevens et al. (1999). Stevens et al. found that a 1.2 $\times 10^{12} M_\odot$ galaxy moving with Mach number $\gtrsim 2$ and with a replenishment rate of about 5 $M_\odot$ yr^{-1} will drive a bow shock of radius $\gtrsim$ 30 kpc. Accounting for gravitational acceleration of ICM gas by a massive halo resembles the treatment of the well known Bondi-Hoyle accretion (see e.g. Balsara et al. 1994; Stevens et al. 1999), but the scale of an accretion-driven shock is smaller than that of a bow shock driven by a supersonically moving halo baryonic barier (because $M_h > 1$). We neglect the difference between the halo Mach number M_h and the bow-

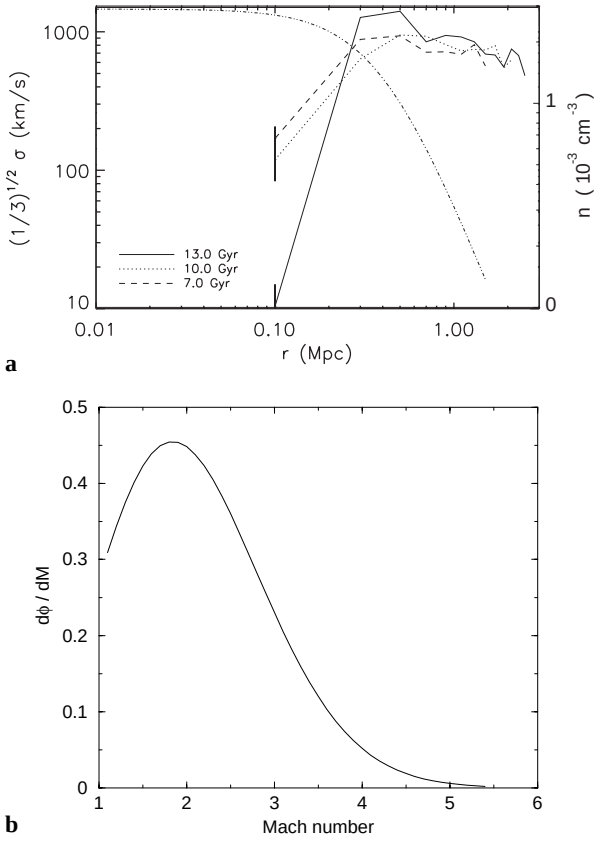

Fig. 1. a Mass-weighted halo velocity dispersion profile from N-body simulations by Okamoto & Habe (1999), together with the ICM radial density profile used in this paper. **b** Differential probability distribution of bow-shock Mach numbers for a virialized halo ensemble at $r \simeq 0.4$ Mpc (for details see Sect. 2).

shock Mach number M_{sh}. We do account for the dependence of the bow-shock opening angle on the halo Mach number.

The probability distribution of Mach numbers M_{sh} of bow shocks created by a virialized halo ensemble with velocity dispersion σ in a galaxy cluster with ICM temperature T follows from Eq. (1). The shock distribution also depends upon whether the ICM pressure is dominated by a nonrelativistic plasma or by a relativistic component (e.g. cosmic rays). Fig. 1b presents the shock distribution function, calculated for a distance of ~ 0.4 Mpc from the centre of a cluster of age 13 Gyr as simulated by Okamoto & Habe (1999). A gas temperature of 10^8 K was assumed (cf. Frenk et al. 1999).

3. Electron acceleration by a halo bow shock

The collisionless bow shocks produced by supersonic motions of halos in the ICM are sites of nonthermal particle generation. Direct observations in the interplanetary medium indicate that both electrons and nuclei are indeed accelerated efficiently by the Earth's bow shock (e.g. Blandford & Eichler 1987; Jones & Ellison 1991). Electron acceleration events were detected in interplanetary shocks of moderate Mach numbers (e.g. Tsurutani & Lin 1985; Shimada et al. 1999). Although the statistics of such observations is limited, they are the most direct evidence for diffusive shock acceleration to operate at moderate Mach numbers.

Electron kinetics in supercritical collisionless shocks was modelled by Bykov & Uvarov (1999). They showed that strong MHD fluctuations generated by kinetic instabilities of ions are responsible for heating and pre-acceleration of nonthermal electrons on a very fine scale (of the order of several hundreds of inertial lengths) in the vicinity of the viscous jump of a collisionless shock. Their model was successfully applied to describe the nonthermal electron fluxes observed near interplanetary shock waves, where typical sonic Mach numbers are $\sim$3. The electron acceleration model was also used in simulations of nonthermal emission from an evolved supernova remnant interacting with a molecular cloud (Bykov et al. 2000). We have used here a numerical code based on this kinetic model, accounting for diffusion and advection of electrons in the halo plasma as well as for Coulomb and synchrotron losses. The nonthermal emission processes are described in detail in Bykov et al. (2000).

3.1. The kinetic equation & the three zones

There are three zones in our model: the pre-shock ICM (zone I), the shock transition region (II), and the post-shock flow (III), where nonthermal emission from shock-accelerated particles originates. In order to calculate spectra of nonthermal electrons in these regions, we used the following kinetic equation for the nearly-isotropic distribution function $N_i(z,p,t)$ (i = I – III):

$$\frac{\partial}{\partial t}\,N_i + u_i(z)\,\frac{\partial}{\partial z}\,N_i - \frac{p}{3}\,\frac{\partial}{\partial p}\,N_i\,\left(\frac{\partial}{\partial z}\,u_i\right) = k_i(p)\,\frac{\partial^2 N_i(z,p)}{\partial z^2} + \frac{1}{p^2}\,\frac{\partial}{\partial p}\,p^2 D_i(p)\,\frac{\partial N_i}{\partial p} + + \frac{1}{p^2}\,\frac{\partial}{\partial p}\,(p^2 L_i(p)\,N_i). \quad (2)$$

This Fokker-Planck-type equation takes into account diffusion and advection [bulk velocity $u_i(z)$] of electrons in phase space due to interactions with MHD waves and the large-scale MHD flow (Bykov & Toptygin 1993). $L_i(p)$ is the momentum loss rate of an electron due to Coulomb collisions in a partially ionized plasma (e.g. Ginzburg 1979). The momentum diffusion coefficient $D(p)$ is responsible for second order Fermi acceleration and $k_i(p)$ is the fast particle spatial diffusion coefficient. For low-energy electrons ($E < E_c$), Coulomb and ionization losses are important everywhere except for the narrow shock transition region (II), where acceleration is fast enough to overcome losses and where nonthermal electron injection occurs. The characteristic energy E_c depends on the plasma density, the ionisation state, the magnetic field, and the diffusion coefficient $k_i(p)$. The corresponding momentum p_{ci} can be defined as the point where the last two terms in Eq. (2) are equal.

A plausible approximation for the diffusion coefficients $k_i(p)$ was adopted here:

$$k_i(p) = k_{i0} \begin{cases} 1, & p_T \le p \le p_* \\ vp^a/v_* p_*^a, & p_* \le p \le p_{**} \\ cp^2/(p_{**}^{2-a} p_*^a v_*) & p \ge p_{**}, \end{cases} \quad (3)$$

where p_T is the momentum of the upstream thermal electrons. p_* and p_{**} are defined below. We used the standard relation for the momentum diffusion coefficient, $D_i(p) = p^2 w_i^2/9k_i(p)$ (e.g. Berezinsky et al. 1990).

In the low-energy regime, $p \le p_*$, particle transport is dominated by large-scale turbulent advection (Bykov & Toptygin 1993). The large-scale turbulence is due to stochastic MHD plasma motions (from shock-wave instabilities) on scales Λ longer than the particle mean free path for resonant scatterings. The large-scale vortex rms-velocity w_i is typically a fraction of the bulk speed u_i. The spatial diffusion is energy independent below p_* and $k_{i0} \sim w_i\Lambda$.

For $p_* \le p \le p_{**}$, electrons are scattered by resonant MHD waves generated by the streaming instability of shock-accelerated particles (e.g. Blandford & Eichler 1987). In this case w_i is close to the Alfvén velocity v_a and the electron diffusion coefficient $k_i(p)$ corresponds now to resonant wave-particle interactions. If the power spectrum of magnetic field fluctuations of the Alfvénic turbulence is approximated by $dB_k^2/dk \sim k^{-\theta}$, then the power-law index a in Eq. (3) is related to the θ as $a = 2-\theta$. The MHD-turbulence spectral index θ depends on the source of the turbulence. For the galactic interstellar medium, where the energy balance is determined by supernova explosions, winds from massive stars, and infall of high-velocity clouds, θ is expected to be in the range 1.5–2 (Bykov 1988). But galaxies moving with $M_h \gtrsim 2$ will suffer efficient ram-pressure stripping, which can change the turbulence scenario because of the lack of Population I stars. Therefore, we are using here a turbulence model which adopts large-scale magnetic field fluctuations due to streaming instabilities near the extended halo bow shock. In this case $a \sim 1$ and the diffusion coefficient at $p \ge p_*$ can be written as $k_i(p) = (1/3)\eta_i v r_e(p)$, where $r_e(p)$ is the electron gyroradius (cf. Jones & Ellison 1991). The parameter η_i determines the scattering "strength". Strong scattering (Bohm limit) corresponds to $\eta_i \sim 1$. We have used here a conservative value, $\eta_i \sim 100$. The momentum p_* follows from $(1/3)\eta_i v r_e(p_*) = w_i\Lambda$. The diffusion model with $a = 1$ was successfully used for modelling of electron acceleration by interplanetary shock waves of moderate Mach numbers by Bykov & Uvarov (1999).

3.2. Characteristics of the three zones

3.2.1. Zone I

In this pre-shock region of the shock (ICM), we assume a highly ionized plasma of temperature $T_8 \sim 1$ and a gas number density depending on radial distance r from the cluster center (see e.g. Sarazin 1988):

$$n_g = n_0 \left[1 + \left(\frac{r}{r_c}\right)^2\right]^{-3\beta/2}, \quad (4)$$

where $n_0 \sim 10^{-3}$ cm^{-3} and r_c is the cluster core radius, which is typically $\gtrsim 0.3$ Mpc. The results from our calculations as shown in Figs. 4 and 5 are focussed on the Coma cluster, assuming a King-type density profile as described by Eq. (4) with β = 0.75, $r_c = 0.4$ Mpc, and $n_0 = 2.9 \times 10^{-3}$ cm^{-3} (Briel et al. 1992). The Alfvén velocity is typically ~ 10 km s^{-1}. We adopted a conservative diffusion model where $k_I(p)$ has a = 1 and applied a moderate scattering strength, $\eta_I \gtrsim 100$.

3.2.2. Zone II

In this shock transition region, injection and heating of electrons occur due to nonresonant interactions with strong MHD fluctuations generated by ion flow instabilities. The scale of the collisionless shock transition region is about 10^{12} cm, which is much smaller than the scales of all other regions important for acceleration and emission. Highly fluctuating magnetic fields of rms amplitude above a few μG are present, being responsible for the formation and structure of the collisionless shock waves (see Fig. 1 of Bykov & Uvarov 1999). Fluctuating magnetic fields in the transition zone are the main agent of dissipative collisionless relaxation in the shock wave.

The momentum diffusion coefficient is given by

$$D_{II}(p) \approx p^2\, \bar{C}\, \left(\frac{\delta B}{B_0}\right)^2 \left(\frac{v_a}{v}\right)^2 \left(\frac{v}{l_i}\right), \quad (5)$$

(Bykov & Uvarov 1999), where $\bar{C} \sim 1$ and $\delta B \gtrsim B_0$. The Alfvénic Mach number of the shock M_a is $\gtrsim 30$, but the sonic Mach number is much lower, typically below 3.5. Thus, the effect of accelerated particle pressure on the shock structure is expected to be not important. In this scenario, we calculated the parameter values for the electron momentum space diffusion coefficients and the velocity profile in the shock transition region from a hybrid simulation of moderate Mach number shock structure (Bennett & Ellison 1995). Coulomb losses are overcome by strong Fermi acceleration in this narrow shock transition region.

3.2.3. Zone III

This post-shock layer has at least about 3×10^{20} cm^{-2} of highly ionized plasma with an initial density of about δ times that of the pre-shock region (where δ is the shock compression ratio). The Alfvén velocity in the highly ionized portion of this zone is somewhat higher than that in the pre-shock region, namely ~ 100 km s^{-1}. Large-scale vorticity with an amplitude $\lesssim 100$ km s^{-1} on parsecs scale may be present here due to local shock instabilities. This would dominate the low-energy electron propagation. Coulomb losses are important in this post-shock layer for electrons with energies below the GeV regime. These losses and Fermi shock acceleration were treated simultaneously. Inverse-Compton and synchrotron losses of relativistic electrons were accounted for following Ginzburg (1979); bremsstrahlung energy losses are relatively unimportant here. A diffusion coefficient as described by Eq. (3) was applied, with $k_{i0} = 5 \cdot 10^{23}$ cm^2 s^{-1} and a = 1. We used $E(p_*) \sim 80$ keV and

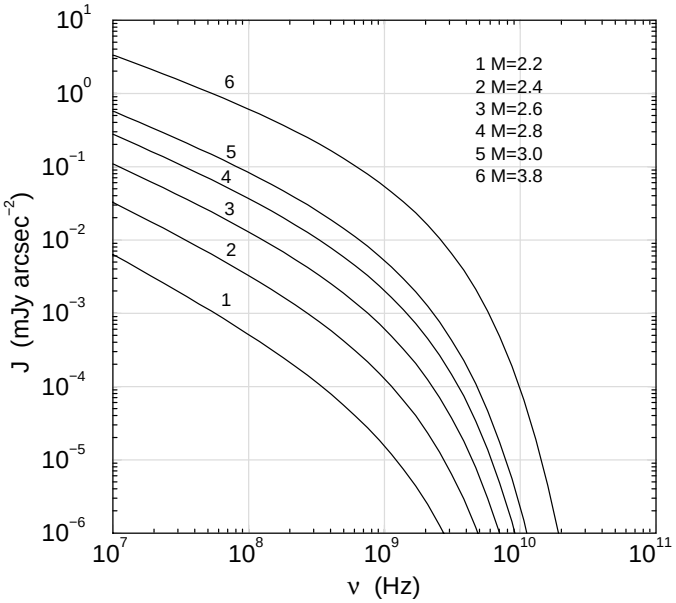

Fig. 2. Radio synchrotron spectrum of a fast moving halo, resulting from nonthermal electron production by a bow shock of Mach number M with direct injection of electrons from the ICM thermal pool. See text for details on parameter values.

$E(p_{**}) \sim 0.5$ GeV, as typically expected for resonant scattering in the post-shock plasma.

4. Nonthermal cluster emission

4.1. Individual halos

We have determined the electron distribution function for different bow-shock Mach numbers and calculated the associated nonthermal emission for individual halos. As the accelerated electrons evolve through the post-shock structure, including possibly dense parts (a galactic disk may be present, or just clouds embedded in the halo), the local emissivities from bremsstrahlung, inverse-Compton radiation, and synchrotron radiation were calculated. Then we integrated these emissivities over the post-shock halo structure.

The results shown here in Figs. 2 and 3 assume an ICM density in the incoming flow of 10^{-3} cm^{-3}, an ICM temperature of 10^8 K, and an ICM magnetic field of 0.1 μG. We used a cluster gas density profile as described above (Sect. 3.2.1), corresponding to the Coma cluster. Galactic photoelectric absorption of X-ray emission was simulated with an adopted line-of-sight column density N_H of $2 \cdot 10^{20}$ cm^{-2}, using cross sections from Morrison & Mccammon (1983).

The radio synchrotron emission was calculated using the standard formulae given by Ginzburg (1979). Fig. 2 shows the synchrotron spectrum of a halo for bow shocks of different Mach numbers. The differential cross sections of electron – ion bremsstrahlung emission (Bethe-Heitler formulae) were taken from Akhiezer & Berestetsky (1957) taking into account the Elwert factor, which is important for modelling the keV emission. The electron – electron bremsstrahlung contribution to the

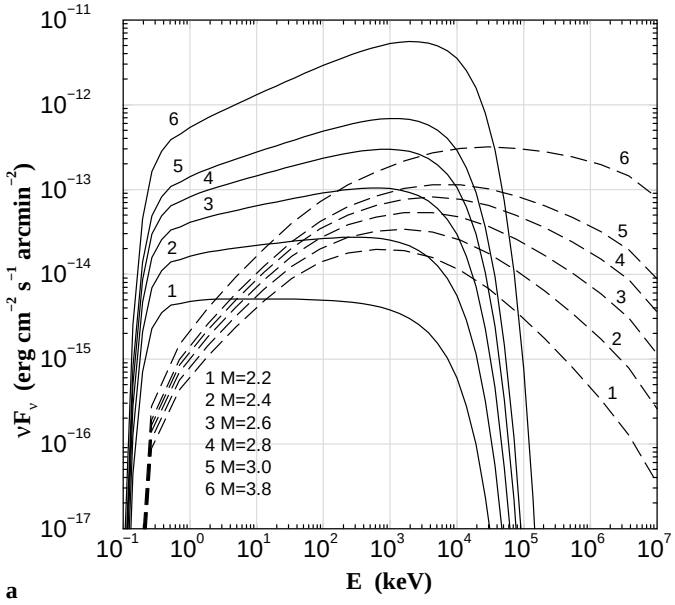

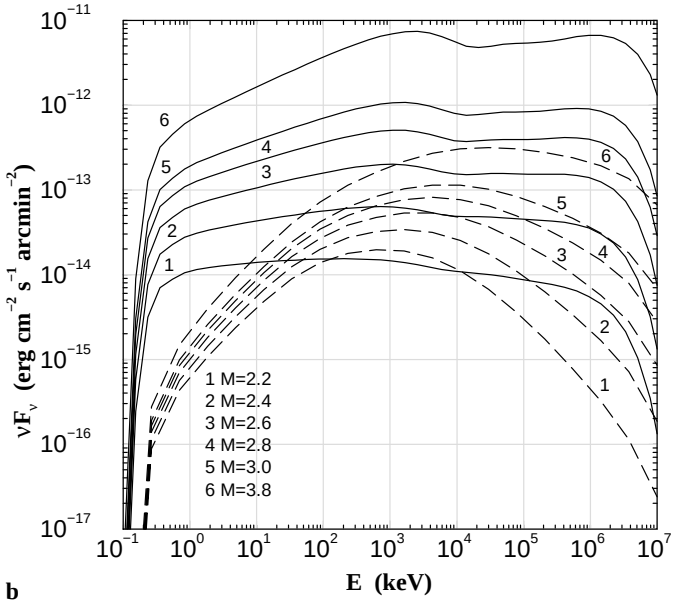

Fig. 3. a X-ray/γ-ray spectrum of a supersonically moving halo of Mach number M. *Dashed line:* bremsstrahlung. *Full line:* inverse-Compton emission. The latter was calculated under the assumption of a photon field that consists of the cosmic microwave background only. **b** The same, but under the assumption that the halo radiation field is the same as Mathis et al. (1983) evaluated for the inner Milky Way. See text for details on parameter values.

γ-ray emissivity was calculated using cross sections derived by Haug (1975). For the inverse-Compton emissivity, we used two different descriptions of the background photon field, namely a pure cosmic microwave background field and a field as present in the (inner) Milky Way (from Mathis et al. 1983). This local radiation field can be constrained from *EGRET* γ-ray upper limits (see Sect. 5). Fig. 3 presents X-ray/γ-ray spectra of a halo for different Mach numbers.

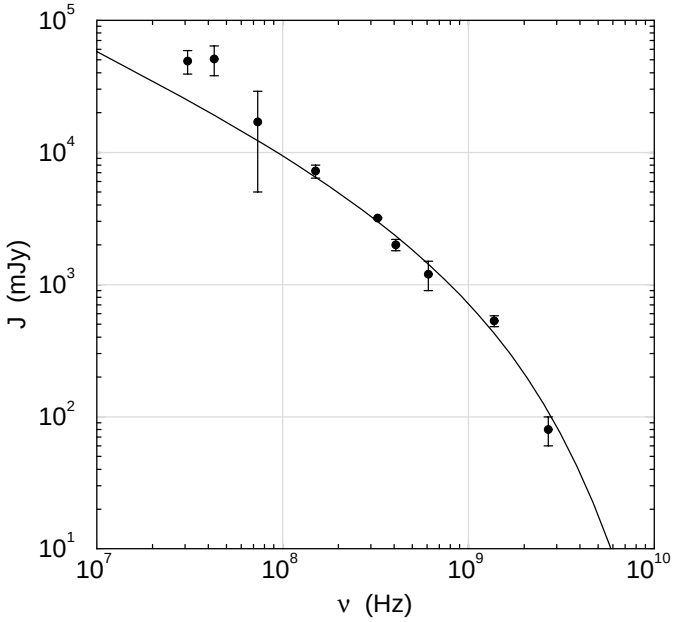

Fig. 4. The modelled radio spectrum of a cluster, after weighting individual halo spectra (Fig. 2) with the bow-shock Mach number distribution (Fig. 1b) and a Press-Schechter type halo mass distribution for a cluster as simulated by Okamoto & Habe (1999). The model parameters are typical for the Coma cluster, of which flux measurements are shown (Giovannini et al. 1993). The normalization of the model spectrum corresponds to a contribution of about 25 halos.

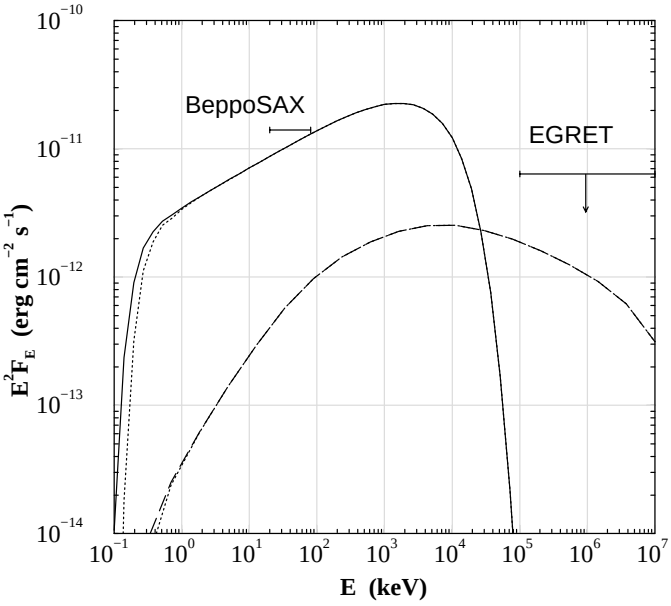

Fig. 5. The modelled (non-thermal) X-ray/γ-ray spectrum of a cluster, after weighting individual halo spectra (Fig. 3a) with the bow-shock Mach number distribution (Fig. 1b) and a Press-Schechter type halo mass distribution for a cluster as simulated by Okamoto & Habe (1999). *Dashed line:* bremsstrahlung. *Full line:* inverse-Compton emission (microwave background scattering). The model parameters are typical for the Coma cluster. The Coma-cluster 20–80 keV flux obtained from *BeppoSAX* observations is shown (Fusco-Femiano et al. 1999; including thermal emission) together with the 2σ upper limit from *EGRET* observations above 100 MeV (Sreekumar et al. 1996). The normalization of the model spectrum corresponds to a contribution of about 25 halos.

4.2. Integrated cluster emission

The cluster spectrum can be obtained by combining the emission from individual galactic halos at the same age. This requires weighting with the halo velocity distribution function, as derived from N-body simulations, and with the mass function of galaxies in the cluster. Because of *i)* the radial increase of the halo velocity dispersion and *ii)* the radial decrease of the ICM gas density (both shown in Fig. 1), the integrated nonthermal emission from supersonically moving halos will show an annular distribution at about 0.3–1 Mpc distance from the cluster center (depending on the cluster mass). Our modelling predicts that only those clusters will have significant nonthermal emission for which the right combination of halo velocity dispersion and local ICM temperature allows $\sigma \gtrsim c_s$. This will be outside the central region where halos are expected to be slowed down by dynamical friction.

Fig. 4 presents the radio synchrotron spectrum of a cluster after averaging over the Mach-number probability distribution (Fig. 1b) and the Press-Schechter type halo mass function in a cluster as simulated by Okamoto & Habe (1999). Fig. 5 shows the corresponding inverse-Compton and bremsstrahlung νF_ν spectra. As the model parameters we have used can be considered typical for the Coma cluster, we have included flux measurements for this cluster in both figures. The modelled radio synchrotron emission (Fig. 4) depends upon the magnetic field of the individual halos, for which we used $0.07\,\mu$G (see Sect. 5.1). We find that $\sim$ 25 contributing halos are required. Observational constraints and implications are addressed below in further detail.

5. Discussion

5.1. Radio emission

High-resolution radio observations can provide an important test for models of particle acceleration in clusters. It was established long ago (see e.g. the review by Hanisch, 1982) that some clusters contain a large (~ 1 Mpc) diffuse radio halo that is not associated with any single active galaxy, but rather with the cluster as a whole. Schlickeiser et al. (1987) considered different scenarios for the origin of the diffuse radio emission from the Coma cluster and found that a remarkably good fit to the observed radio spectrum is provided by an *in-situ* acceleration model. The model we discuss here also belongs to the class of *in-situ* acceleration models, but we assume that the observed emission is due to an ensemble of sources — supersonically moving halos — rather than truly diffuse emission. The velocity distribution of halos, as derived from N-body simulations, indicates that indeed a substantial number of halos with bow shocks of $M_h \gtrsim 2$ may be present. These will have relatively steep radio spectra up to a few GHz (index of ~ 1) and tails of about 30 kpc. The superposition of such sources would then

produce the low-brightness diffuse radio glow from a cluster in the scenario considered here.

The low surface brightness complicates imaging of extended diffuse radiation. Giovannini et al. (1993) reported that relatively few clusters have unambignously detected extended emission [A1367, A1656 (Coma C), A2255, A2256, and A2319]. The Effelsberg radio survey of 34 Abell clusters showed indications for extended emission in only two clusters, A665 and A2152, at 2.7 GHz (Andernach et al. 1988). The subtraction of point sources introduces an additional uncertainty. The actual integrated radio flux that should be compared with our model may be higher (i.e. part of the ensemble of halos producing the extended emission may have been removed). Therefore, as the magnetic field in the halos determines the synchrotron emission in our model, the value of 0.07 μG used in Fig. 4 may actually be a lower limit for the Coma-cluster halos.

As the electron acceleration results from supersonically moving halos that are subject to efficient stripping (e.g. Stevens et al. 1999), the magnetic field may be lower than in normal galactic halos. Although we are not formally constraining the magnetic field of the ICM, it is expected to be of the order of the field for a stripped halo in the outer regions of the cluster. For those clusters of which hard X-ray emission has been reported from *BeppoSAX* observations, namely A1656 (Coma) (Fusco-Femiano et al. 1999), A2199 (Kaastra et al. 1999), and A2256 (Fusco-Femiano et al. 2000), we can place upper limits on the halo magnetic fields by assuming a certain statistical distribution. If halos moving with Mach numbers $\lesssim 3$ dominate, the ensemble is sufficiently stripped to have magnetic fields close to that in the ICM and the upper limit on the magnetic field in these clusters is about 0.1 μG for the assumed cluster gas density and halo velocity distribution. This is consistent with values advocated in other studies (Rephaeli et al. 1994; Völk & Atoyan 1999). Further discussion on the magnetic field is given in the following section. The non-detection with *BeppoSAX* of a hard excess for the rich cluster A2319 at $z = 0.056$, which is known to be a source of diffuse radio emission, can be used to set a lower limit on the ICM field of $\sim$0.04 μG (Molendi et al. 1999).

5.2. X-ray and gamma-ray emission

The model spectra in Fig. 5 are compared with the *BeppoSAX* observation of the Coma cluster (Fusco-Femiano et al. 1999; $\sim 2.2\times10^{-11}$ erg cm^{-2} s^{-1}, 20–80 keV) and the (2σ) *EGRET* upper limit (Sreekumar et al. 1996; 4×10^{-8} photon cm^{-2} s^{-1} above 100 MeV). No thermal contribution has been subtracted from the BeppoSAX measurement.

We assumed a modest matter depth in the halos ($\sim 3 \times 10^{20}$ cm^{-2}) which is close to the shocked ICM matter depth. The upper curve (IC emission) presented in Fig. 5 is not sensitive to the matter distribution in the halos. The low-energy (below $\sim$1 MeV) branch of the lower curve (bremsstrahlung emission) is only marginally influenced, even if the available amount of matter in the halos would be significantly less. This is because of diffusive propagation of low-energy electrons. The bremsstrahlung emission above $\sim$10 MeV can be roughly linearly scaled with the halo matter depth available.

Halos are difficult to detect individually with current hard X-ray instruments, but can produce a granular appearance of cluster emission that may already be observable by *Chandra* and *XMM*. This holds in particular for extended halos in the outer regions of low-redshift clusters of temperatures below about 7 keV. Stevens et al. (1999), on the basis of their model calculations, pointed out the possibility of observing thermal emission from extended bow shocks and bright tails of supersonically moving galaxies in clusters with *Chandra* and *XMM*.

The upper limit imposed by *EGRET* observations of the Coma cluster (Fig. 5) implies that only a small fraction of the halos ($\lesssim 10\%$) can have a radiation field like Mathis et al. (1983) derived for the inner Milky Way. We note that our modelled X-ray/γ-ray νF_ν cluster spectra peak in the COMPTEL energy regime at 1–10 MeV, but no dedicated cluster study using COMPTEL data has been performed yet.

In the hard X-ray regime, we see (Fig. 3) that IC emission dominates bremsstrahlung, unless the Mach number is low. The latter may be the case if mass replenishment is not sufficient to compensate the stripping effect for halos of high Mach number. An important advantage of models in which the hard X-ray emission is dominated by IC emission is the high energetical efficiency in comparison to bremsstrahlung models (e.g. Sarazin & Kempner 2000). On the other hand, IC models require magnetic field strengths of about 0.1 μG (as discussed above), which is below that from equipartition and that determined from Faraday rotation toward individual radio galaxies under the assumption of a highly tangled cluster magnetic field. Our model implies relatively low values for the ICM magnetic field outside the central 0.3–0.4 Mpc region only. This can be consistent with rotation measure observations by Kim et al. (1991) if the cluster-scale magnetic field reversal length is rather large, namely $\gtrsim 250$ kpc. Studies of the magnetic field structure in the outer regions of clusters are important to distinguish between IC and nonthermal bremsstrahlung models. High magnetic fields would require parameters for the diffusion model [Eq. (3)] that suppress efficient acceleration of relativistic electrons. Hard X-ray tails would then be dominated by nonthermal bremsstrahlung emission. The energetical requirements would be stringent.

5.3. Perspectives for INTEGRAL and GLAST

The modelled photon flux around 100 keV from clusters like Coma, A2199, and A2256 can be observed with *INTEGRAL*. At 1 MeV, the modelled flux ($\sim 10^{-5}$ photon cm^{-2} s^{-1} MeV^{-1}) is below the expected sensitivity. Important constraints, however, can in principle be obtained by combining observations of e.g. a dozen rich clusters of redshifts $z \leq 0.05$. The sensitivity of the future *GLAST* experiment above 100 MeV appears to be sufficient to detect bremsstrahlung at these energies, which is expected at a level of $\sim 10^{-8}$ photon cm^{-2} s^{-1}. At least highly constraining limits can be obtained.

5.4. Merging and accretion shocks

The mechanism considered here may dominate (or at least substantially contribute to) the nonthermal emission of an evolved relaxed cluster. A2199 at z = 0.03 could be a good example of such a relaxed cluster, with a moderate cooling flow and a quite symmetrical X-ray brightness distribution (e.g. Markevitch et al. 1999), without indications for a merging process. In A2256, however, a merger process may be ongoing (Molendi et al. 2000). The same holds for some other clusters, showing elongated structures, like A2319 (e.g. Feretti et al. 1997) and A3667 (e.g. Roettiger et al. 1999). The ongoing merger of clusters may launch a large-scale accretion shock (e.g. De Young 1992; Schindler & Müller 1993; Roettiger et al. 1999). This accretion shock can be an efficient source of accelerated electrons and nonthermal emission (e.g. Roettiger et al. 1999; Sarazin 1999). We note that our modelling of electron acceleration by shocks and nonthermal emission spectra from individual shocks of a given Mach number can be applied to the accretion shock scenario as well, after appropriate scaling of the gas number density.

6. Summary and conclusions

We have presented a model of nonthermal emission from rich clusters of galaxies, where bow shocks of moderately supersonically moving galactic halos produce accelerated particles and then radio, X-ray, and γ-ray emission. Using results from global N-body simulations of the dynamical evolution of galactic halos in rich clusters and a kinetic model of energetic electron acceleration, we calculated the spectra and the spatial distribution of nonthermal emission.

A comparison with observations shows good agreement. Our modelling indicates that the temporal evolution is sensitive to the cluster dynamical evolution model and we find that sensitive spatially resolved observations of nonthermal emission (radio, EUV, X-ray, and γ-ray) can constrain cluster-evolution simulations. Such observations will also provide a valuable tool to study halo velocity dispersion profiles in clusters and constrain the magnetic field, the halo radiation field, and the ram-pressure stripping efficiency, which are important for evolution studies of the baryonic component in the intra-cluster medium. We have presented the spectra of nonthermal emission from shock waves of different strengths, which can be used for modelling of emission from large-scale accreting shocks in merging clusters as well.

Acknowledgements. This work was supported by INTAS grant 96-0390, INTAS/ESA grant 99-1627, and by a visitors grant to A.M.B. from the Netherlands Organisation for Scientific Research (NWO). A.M.B. acknowledges the traditionally warm hospitality at SRON Utrecht.

References

Andernach H., Han Tie, Sievers A., et al., 1988, A&AS 73, 265
Akhiezer A.I., Berestetsky V.B., 1957, Quantum Electrodynamics. Transl. by Consultants Bureau Inc., Tech. Information Service Ext., Oak Ridge
Balsara D., Livio M., O'Dea P., 1994, ApJ 437, 83
Bennett L., Ellison D.C., 1995, J. Geoph. Res. A100, 3439
Berezinsky V.S., Blasi P., Ptuskin V.S., 1997, ApJ 487, 529
Berezinsky V.S., Bulanov S.V., Dogiel V.A., Ginzburg V.L., Ptuskin V.S., 1990, Astrophysics of Cosmic Rays. North Holland, Amsterdam
Bertschinger E., 1999, ARA&A 36, 599
Blandford R., Eichler D., 1987, Physics Reports 154, 2
Blasi P., 1999, ApJ 525, 603
Blitz L., Spergel D.N., Teuben P.J., Hartmann D., Burton W.B., 1999, ApJ 514, 818
Bowyer S., Berghöfer T.W., Korpela E., 1999, ApJ 526, 592
Briel U.G., Henry J.P., Böhringer H., 1992, A&A 259, L31
Bykov A.M., 1988, SvA Lett. 14, 60
Bykov A.M., Toptygin I.N., 1993, Physics Uspekhi 36, 1020
Bykov A.M., Uvarov Yu.A., 1999, JETP 88, 465
Bykov A.M., Chevalier R.A., Ellison D.C., Uvarov Yu.A., 2000, ApJ 538, 203
De Young D.S., 1992, ApJ 386, 464
Enßlin T.A., Biermann P.L., 1998, A&A 330, 90
Enßlin T.A., Lieu R., Biermann P.L., 1999, A&A 344, 409
Ferretti L., Giovannini G., Böhringer H., 1997, New Astron. 2, 501
Frenk C.S., White S.D.M., Bode P., et al., 1999, ApJ 525, 554
Fusco-Femiano R., Dal Fiume D., Feretti L., et al., 1999, ApJ 513, L21
Fusco-Femiano R., Dal Fiume D., de Grandi S., et al., 2000, ApJ 534, L7
Gaetz T.J., Salpeter E.E., Shaviv G., 1987, ApJ 316, 530
Ghigna S., Moore B., Governato F., Lake G., Quinn T., Stadel J., 1998, MNRAS 300, 146
Ginzburg V.L., 1979, Theoretical Physics and Astrophysics. Pergamon Press, Oxford
Giovannini G., Feretti L., Venturi T., Kim K.-T., Kronberg P.P., 1993 ApJ 406, 399
Hanisch R.J., 1982, A&A 116, 137
Haug E., 1975, Z. Naturforsch. 30a, 1099
Hwang C.-Y., 1997, Sci 278, 1917
Jones F.C., Ellison D.C., 1991, Space Sci. Rev. 58, 259
Kaastra J.S., Lieu R., Mittaz J.P.D., et al., 1999, ApJ 519 L119
Kempner J.C., Sarazin C.L., 2000, ApJ 530, 282
Kim K.-T., Trimble P.C., Kronberg P.P., 1991, ApJ 379, 80
Klypin A., Gottlöber S., Kravtsov A.V., Khokhlov A.M., 1999a, ApJ 516, 530
Klypin A., Kravtsov A.V., Valenzuela O., Prada F., 1999b, ApJ 522, 82
Lieu R., Ip W.-H., Axford W.I., Bonamente M., 1999, ApJ 510, L25
Markevitch M., Vikhlinin A., Forman W.R., Sarazin C.L., 1999, ApJ 527, 545
Mathis J.S., Mezger P.C., Panagia N., 1983, A&A 128, 212
Molendi S., De Grandi S., Fusco-Femiano R., et al., 1999, ApJ 525, L73
Molendi S., de Grandi S., Fusco-Femiano R., 2000, ApJ 533, L43
Moore B., Ghigna S., Governato F., et al., 1999, ApJ 524, L19
Morrison R., Mccammon D., 1983, ApJ 270, 119
Okamoto T., Habe A., 1999, ApJ 516, 591
Rees M.J., 1986, MNRAS 218, 25p
Reimer O., 1999, In: Proc. 26th ICRC Salt-Lake City, OG 2.4.15
Rephaeli Y., 1979, ApJ 227, 364
Rephaeli Y., Ulmer M., Gruber D., 1994, ApJ 429, 554

Rephaeli Y., Dermer C.D., 1997, In: Dermer C.D., Strickman M.S., Kurfess J.D. (eds.) Proc. 4th Compton Symposium, p. 271
Rephaeli Y., Gruber D., Blanco P., 1999, ApJ 511, L21
Roettiger K., Burns J.O., Stone J.M., 1999, ApJ 518, 603
Roland J., 1981, A&A 93, 407
Sarazin C.L., 1988, X-ray emission from clusters of galaxies. Cambridge University Press, Cambridge
Sarazin C.L., Lieu R., 1998, ApJ 494, L177
Sarazin C.L., 1999, ApJ 520, 529
Sarazin C.L., Kempner J.C., 2000, ApJ 533, 73
Schindler S., Müller E., 1993, A&A 272, 137
Schlickeiser R., Sievers A., Thiemann H., 1987, A&A 182, 21
Shimada N., Terazawa T., Hoshino M., et al., 1999, Ap&SS 264, 481
Sreekumar P., Bertsch D.L., Dingus B.L. et al., 1996, ApJ 464, 628
Stevens I.R., Acreman D.M., Ponman T.J., 1999, MNRAS 310, 663
Tsurutani B.T., Lin R.P., 1985, J. Geoph. Res. 90, 1
Völk H., Aharonian F.A., Breitschwerdt D., 1996, Space Sci. Rev. 75, 279
Völk H., Atoyan A.M., 1999, Astropart. Phys. 11, 73
White D.A., Jones C., Forman W., 1997, MNRAS 292, 419
White S.D.M., Rees M.J., 1978, MNRAS 183, 341